Nuclear Instruments and Methods in Physics Research A270 (1988) 126-139
North-Holland, Amsterdam

A MONTE CARLO CODE FOR A TIME PROJECTION CHAMBER *

Ming-Jen YANG **

Los Alamos National Laboratory, Los Alamos, NM 87545, USA

Received 7 January 1988

A Monte Carlo code was written to simulate the data collected in a time projection chamber that was used to measure the positron spectrum of muon decay. The computer code traced positrons through the detector, taking into account the nonuniformity of the magnetic field and other known systematic effects, and generated coordinates along simulated trajectories to give an accurate description of the acceptance-resolution function of the spectrometer. The *event topology*, i.e., the geometry of the positron trajectory, generated by the Monte Carlo program was compared with that of the experimental data. This comparison indicated a positive ion effect, which was subsequently modeled and incorporated in the simulation. The magnitude of this effect was determined on the basis of the event-topology comparison without reference to the momentum spectrum.

1. Introduction

A Monte Carlo code was written for the specific purpose of analyzing the data taken in an experiment in which a time projection chamber (TPC) [1,2] had been used to measure the momentum spectrum of the positrons from the decay of positive muons. The spectrometer was designed to accept events over a wide momentum and angular range at a single magnetic field setting.

The data collected by the TPC were used to determine the coordinates of a series of points along the trajectory of the decay positron. The observed momentum and emission angles were determined by fitting these coordinates to a helix. A muon-decay event, as seen by the detector (described in section 2), is displayed in fig. 1. This shows the trajectory of the positron in various projections after the measured coordinates have been fitted to a helix. The observed trajectory, however, does not represent the original momentum of the positron. Account must be taken of physical processes, such as multiple scattering, bremsstrahlung, Bhabha scattering, etc., which cause the positron to lose energy and change trajectory. In addition, systematic effects can affect the coordinate determination and distort the observed trajectory. The observed spectrum must be compared with an expected spectrum based on a theoretical prediction and with the characteristics of the spectrometer taken into account. This requires an

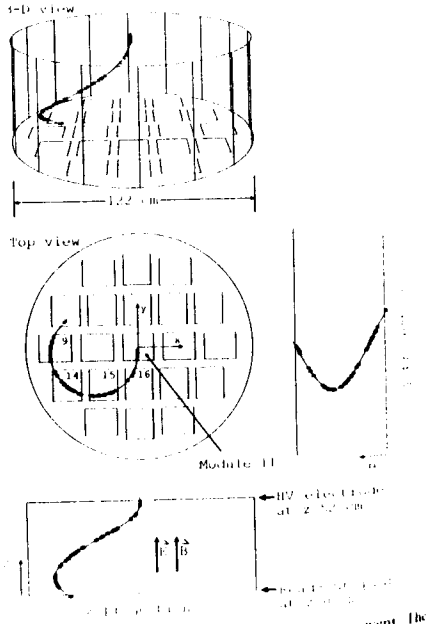

Fig. 1. Example of a reconstructed decay positron event. The coordinates as determined from the analysis of the data were fitted to a helix, shown here in various projections. There were 41 coordinates. The momentum, 47.6 MeV/c, and the cosine of the dip angle equals −0.49 were determined from the helix parameters. The arrangement of the 21 wire chamber modules can be seen in the top view of this figure.

* Submitted in partial fulfillment of the Ph.D. requirements of the Department of Physics, the University of Chicago.

** Also with the Enrico Fermi Institute, the University of Chicago.

0168-9002/88/$03.50

accurate knowledge of the acceptance and resolution functions of the spectrometer over the wide range of momentum and angle covered. These are not simple functions in our TPC, nor was it possible to devise methods for determining them by calibration. The only practical way to generate an expected spectrum from the theory was by means of the Monte Carlo method.

In this paper we show how this was done and how a variety of problems having to do with the experiment were dealt with. In particular, we introduce a method that can be used to gauge the performance of the Monte Carlo code without reference to the resulting spectrum. We have applied this method in studying the systematic effects of the detector. A positive ion effect was found which, when included in the simulation, greatly improved the consistency of the data analysis.

2. The experiment

2.1. Time projection chamber

A schematic view of the experimental apparatus is shown in fig. 2. The main component is the TPC as described by Kinnison [3]. It consists of a drift volume and a wire chamber readout plane. The drift volume is enclosed by a cylindrical fiber-glass canister 122 cm in diameter. A high-voltage electrode 52 cm upstream of the readout plane defines the length of the drift volume and provides an electric field of 160 V/cm. The electrode is made of 1/8 inch copper-clad G-10 plate with a 7 inch diameter hole at the center, through which the decay positrons enter the chamber. The hole is covered with 1/4 mil. aluminum foil to make the electrode electrically complete. A Kapton liner imprinted with a series of copper rings 1 cm apart is attached to the inside wall of the fiber-glass canister. The copper rings define the equipotential surfaces, thus ensuring the uniformity of the electric field within the drift volume. A 6 kG magnetic field is provided by six water-cooled copper coils. The drift volume is filled with a 50% argon and 50% methane gas mixture at just under 600 Torr.

A subsurface muon beam with a momentum of 19.5 MeV/c was used in the experiment. The longitudinal polarization of the muon beam was rotated to the transverse direction by an $E \times B$ separator. The separator also removed beam positrons and allowed only muons with a well-defined momentum to enter the spectrometer. A polarimeter located just before the upstream iron yoke was used to ensure the proper spin rotation angle.

2.2. Target counter

The muons stopped in a 1.64 mm thick, 1 inch diameter scintillation target-counter (provided by A.

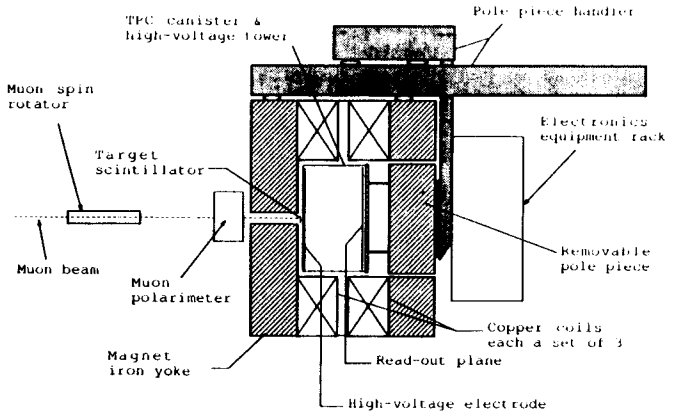

Fig. 2. Time projection chamber: The drift volume is a cylindrical fiber-glass canister, 122 cm in diameter and 52 cm long. It is capped at one end with a high-voltage electrode; at the other end is the read-out plane. The inner lining of the canister is made of Kapton on which copper rings have been printed. These define equipotential surfaces to ensure the uniformity of the electric field. The whole is set in a solenoidal magnetic field of 0.6 T created by water-cooled copper coils set in the iron yoke. Muons enter through a hole in the upstream pole after passing through an $E \times B$ separator used as a spin rotator. They stop in the scintillator target just outside the high-voltage electrode. This electrode has a 7 inch diameter hole covered with a 1/4 inch thick aluminum window through which the decay positrons pass to enter the drift space. The downstream pole can be removed for access to the TPC assembly and its associated electronics at the readout plane.

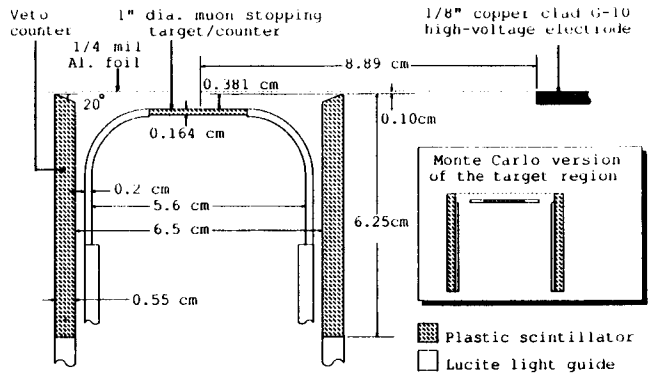

Fig. 3. The muon stopping target scintillator is shown together with the cylindrical light pipe that brings the light to the photomultipliers mounted outside the magnet yoke. The veto counter surrounds the target and its light pipe. The simplified version used in the Monte Carlo simulation is also shown.

Zehnder) at the entrance of the TPC (fig. 2). Fig. 3 is a detailed drawing of the target region. The signal from the target was fed into two discriminators at different discrimination levels. The high-level discriminator output was taken to be the muon stopping signal and the low-level discriminator output, the decay positron signal. The decay positron signal gave the time zero reference for the drift time measurement. The stopping target is surrounded by a cylindrical scintillation veto counter (built by H.J. Ziock). The purpose of this counter was to detect positrons that went in directions leading toward the G-10 portion of the drift high-voltage electrode. The trigger for a muon-decay event was a muon stopping signal, followed by a decay positron signal within a 12 μs timing gate, and the subsequent wire signals from the readout plane within the next 8 μs after the positron signal. An event veto occurred if a veto signal was detected within 50 ns of the decay positron signal.

2.3. Readout plane

The readout plane consists of 21 wire chamber modules as shown in fig. 1. Each module includes a cathode pad plane, a sense wire plane, a pulsing grid plane, a grounded grid plane, and aluminum partitions to isolate

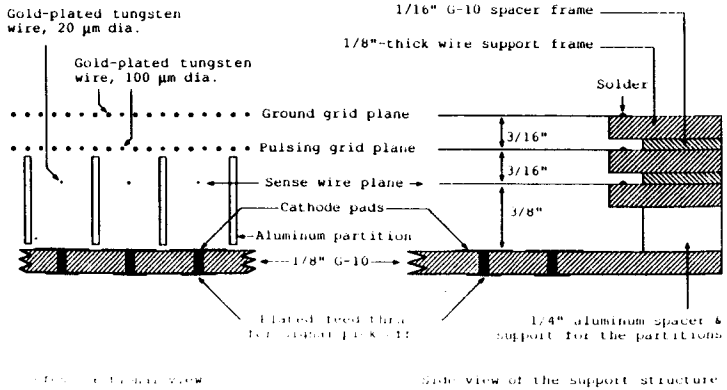

Fig. 4. Cross-sectional view and side view of the readout plane showing the disposition of the grounded grid, the pulsing grid, and the sense wires and their associated cathode pads. Aluminum partitions suppress the crosstalk that would otherwise occur between the regions served by adjacent sense wires.

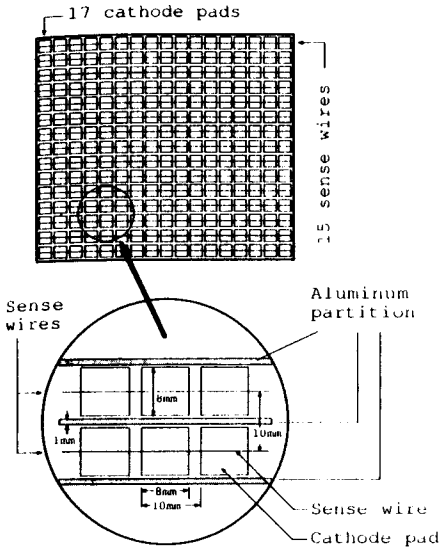

Fig. 5. One of the 21 identical modules of the readout plane. Each module contains 15 sense wires with 17 cathode pads under each.

the sense wires (fig. 4). The wire-pad arrangement is shown in fig. 5. Each module contains 15 sense wires spaced 1 cm apart and 17 cathode pads under each sense wire, also at 1 cm spacing, to provide position information. The pulsing grid was rendered inactive during the experiment by setting it at a constant +75 V.

2.4. Positron trajectory

The function of the TPC was to determine the x, y, z coordinates of a series of points along the trajectory of the decay positron as it traversed the drift volume. The positron followed a helical trajectory, ionizing the gas along the way. The ionization electrons drifted toward the readout plane and ultimately caused the avalanches that produced pulses on the anode wires and induced signals on the underlying cathode pads. The pad signals were digitized at a rate of 20 MHz with flash encoders, known as FADCs (flash analog-to-digital converters), and read out by microprocessors. A detailed description of the operation of the FADCs and the data-acquisition system has been given by Lillberg [4]. One coordinate, either x or y according to the orientation of the molecule, was determined by the location of the sense wire in which the wire signal was seen. The complementary coordinate was determined

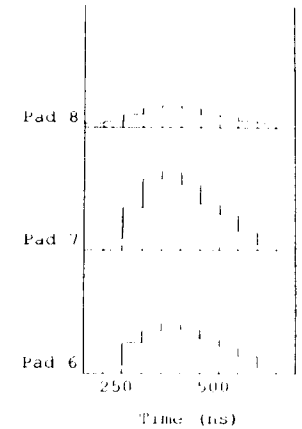

Fig. 6. Typical pulse height structure of the signals induced on a set of cathode pads by a wire hit. The time evolution of the signals as digitized by the flash encoders is displayed. The horizontal axis represents the time.

from an analysis of the pulse height structure as seen on the underlying cathode pads. The cathode pad interpretation technique is widely used in wire-chamber detectors [5]. An example of a set of digitized cathode pad signals is given in fig. 6. The z coordinate was determined from the wire turn-on time by assuming a constant drift velocity (6.8 cm/μs on the average), which was constantly monitored during the experiment. An ^{55}Fe source was used to calibrate the gains of the cathode pad signal amplifiers. Cosmic ray tracks were used to study the positional resolution of the detector.

2.5. Helix fitter

The data written for each event was a set of wire hits. Each wire hit included the wire number, the wire turn-on time, and the associated cathode pad signals. The wire hits were first processed to obtain a set of three-dimensional coordinates. A fit to a helix was then made to obtain the momentum and emission angles of the positron. The helix-fitting routines were written by McKee [6]. The fitting was done in two steps. In the first step all the coordinates were fitted to a circle in the x-y plane. In the second step the azimuthal angles of the x, y coordinates with respect to the center of the circle were calculated. A linear fit to the azimuth-z data points gave the dip angle θ of the positron trajectory. The dip angle is defined as the angle between the direction of the z axis and that of the positron momentum. A typical reconstructed event with 41 coordinates in various projections is shown in fig. 1. The coordinate system used is indicated in the figure. The momentum

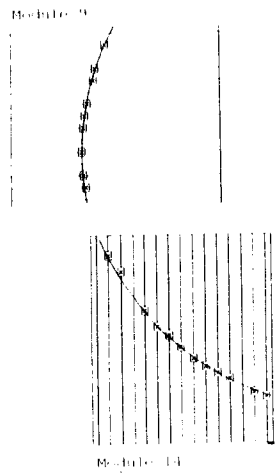

Fig. 7. The x, y projection of the coordinates and the fitted helix (the solid curve), in modules 9 and 14 of the event shown in fig. 1. The track starts at the center of module 11 and then moves successively through modules 16, 15, 14, and 9.

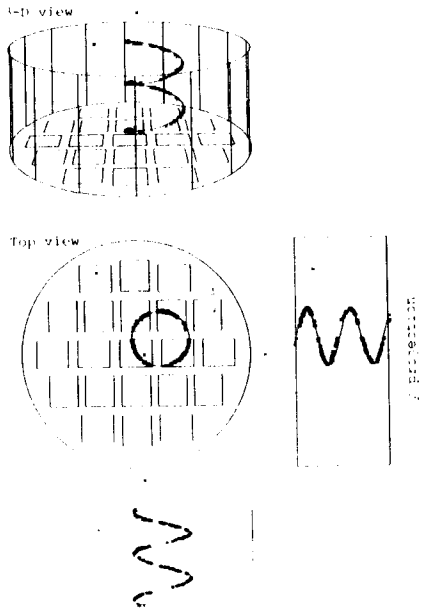

Fig. 8. A multiturn event showing the multihit capability of the TPC. The fit gave a momentum of 28.1 MeV/c and a cos θ of −0.25.

was determined to be 47.6 MeV/c; the cos θ was −0.49. Fig. 7 is a more detailed view of the coordinates in modules 9 and 14 and the fit for the track. (For reference, the track started in module 11, at the center of the read-out plane, and ended in module 9 after passing through module 14.) In fig. 8, we show a multiturn event that demonstrates the multiple-hit capability of the TPC.

2.6. Acceptance-resolution function

The acceptance-resolution function represents our understanding of the detector behavior and is needed for generating an expected spectrum, based on the theoretical prediction, to be compared with that of the observed data. The Monte Carlo data, which give both the initial and fitted momentum of each event, were used to obtain the acceptance-resolution function. The formulation for obtaining this function was due to R.J. McKee and is given as an appendix to this paper to clarify the momentum comparison presented in section 5.2. The subsequent fitting of the positron spectrum to obtain the physics results, i.e., a value for the Michel parameter ρ, is also discussed in the appendix.

3. Monte Carlo simulation

The Monte Carlo simulation described here was done in two stages. The first was the generation of Monte Carlo data. The contributions from physical processes like multiple scattering, bremsstrahlung, Bhabha scattering, Møller scattering, etc., as well as the geometry of the readout plane, were included at this stage. The second stage, the analysis of the simulated data, is described in section 4. All the contributions that were not needed in the first stage were implemented in the second stage. These included the simulation of defective electronics, wire efficiencies, position resolution, and possible fiducial region cuts. In both stages an effort was made to simulate the response of the detector as closely as possible. We fitted the simulated events with the same helix-fitting routines as those used in the analysis of the experimental data, taking care to use exactly the same fitting criteria.

3.1. Simulation of physical processes

Our Monte Carlo simulation made extensive use of the Electron-Gamma-Shower (EGS) computer code. This code was originally developed at the Stanford Linear Accelerator Center (SLAC) and is now maintained by SLAC together with Canadian and Japanese institutions [7]. It is a general-purpose program used to simulate the passage of electrons, positrons, and gamma rays through various materials. The program incorporates all the known physical processes with their known cross sections to account for everything that could and should happen to the particles. Its completeness and validity have been improved over the years. We used the fourth version, EGS4, which we believe includes all the ingredients needed for an accurate simulation.

The interaction of the positron with the material of the TPC results in changes in energy and momentum. Occasionally, extra particles may be generated. Because the cross sections for all processes are well known, the entire course of the shower can be properly taken into account. In the program, the discrete particle generation was simulated above a low-energy cutoff to avoid the problem of dealing with the rapidly increasing cross section at low energies. The contribution from processes generating particles with energies below the cutoff was accounted for by modifying the constants having to do with the energy loss $\mathrm{d}E/\mathrm{d}x$ and the multiple scattering effects. The discrete particle generation simulated, as much as possible, the energy loss fluctuation of the particle along its trajectory. Low cutoff energies of 20 keV for electrons and 1 keV for photons were used.

The amount of multiple scattering and energy loss along the trajectory was updated after every transport step. Because the wires were spaced at 1 cm, the step sizes used ranged from 1 cm to not more than 20 cm. The photons produced by the particles were followed until either their energy was below cutoff or they left the drift volume. No information about individual photons – only a tally of the total photon energy in each event – was output. The knock-on electrons were a source of fluctuation in the $\mathrm{d}E/\mathrm{d}x$. Except for those with relatively large energy, their effect was to modify the simulated trajectory.

All the interaction properties of the materials involved were precalculated by a program called PEGS (for pre-EGS), developed by the writers of the EGS code. PEGS calculates the cross sections for each of the physical processes in the materials specified. Once this has been done, the EGS code need only read in the arrays containing the required cross-section values at initialization.

3.2. Target region simulation

The target region simulation included the scintillator target, the lucite light guide, the veto counter, the material used for wrapping the counter, and the G-10 high-voltage electrode with its 1/4 mil. aluminum foil window. The actual geometry was simplified somewhat in the Monte Carlo simulation (fig. 3). Our purpose in including these nearby materials was to get an assessment of the likelihood of the occurrence of background-related events. This served to guide the choice of a fiducial region to one in which the contribution from background scattering would be minimal.

All positrons were started uniformly and randomly across the target area at a depth of 0.024 cm from the upstream surface. This depth was calculated on the basis of the muon beam momentum of 19.5 MeV/c measured during the experiment. The Monte Carlo simulation began by choosing randomly the initial momentum, the cosine of the dip angle θ, the azimuthal angle ϕ, and the x, y position of muon decay in the target. From this starting position the code tracked the positron until it either left the detector or annihilated with an electron.

3.3. Drift region simulation

In the TPC drift region, the positron moves in a helical path under the influence of the magnetic field. The ionization electrons created along the trajectory drift toward the readout plane under the influence of the electric field. Ideally, with parallel and axial magnetic and electric fields, the arrival of the drift electrons at the readout plane will be an accurate projection of the trajectory. In practice, small deviations from uniformity in either the electric or the magnetic field in the drift region give rise to an $\boldsymbol{E} \times \boldsymbol{B}$ effect. This results in a displacement of the drifting electrons in the x–y plane and complicates the calculation of wire crossings of the particle tracks. The amount of displacement depends on where the ionization originated and can be calculated [8]. This calculation was performed once, and the results were incorporated in two 2-dimensional look-up tables. In one table were stored the radial displacements and in the other, the azimuthal displacements, each as a function of z and the radial distance from the center of the TPC. The amount of displacement at any position was obtained by interpolation.

As the Monte Carlo process followed the particle along its trajectory, the look-up tables were used to project the trajectory onto the readout plane. Thus, it was possible to determine when and where a wire crossing occurred. The transport step size needed to reach the next wire crossing point was calculated on the basis of this projection and the sense wire location.

3.4. Wire hit generation

The Monte Carlo program generated one coordinate each time the simulated track crossed the sensitive volume of a sense wire. Ideally, the wire hit location would be where the track projection cross the sense wire. In reality, the hit location was decided by the portion of the ionization reaching the sense wire first. Because the sensitive volume of each sense wire extended about 0.5 cm on both sides, determining where the hit occurred along the track was not a simple matter. Three factors that complicated this determination were involved: the $\boldsymbol{E} \times \boldsymbol{B}$ effects around the sense

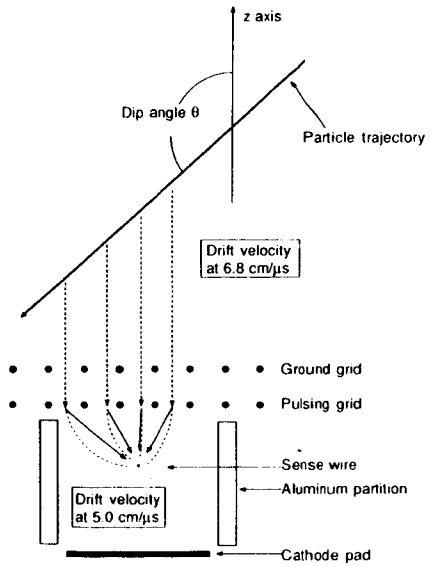

Fig. 9. A sketch of the drift process. The bold solid line represents the track of the charged particle. The ionization electrons created at various locations drift toward the readout plane in their separate courses. A simplified approach – taking the alternative paths indicated by the solid lines with arrow heads pointing toward the sense wire – was used.

wire, the pitch angle of the track with respect to the readout plane, and the clustering of ionization electrons along the particle trajectory.

The velocity and trajectory of drifting electrons change dramatically once the electrons enter the region of the sense wire cell, i.e., the space between the grounded grid and the sense wire. In order to calculate the location on the trajectory from which the ionization electrons will reach the sense wire first, one must know the details of the drift process. At the vicinity of the sense wire, the E field becomes intense and is directed radially outward from the wire, giving rise to a substantial $E \times B$ effect. This effect has been studied by Hargrove [9]. A track having a dip angle of 150° with respect to the z axis and crossing a 1 cm wide sensitive region of the sense wire leaves a segment of ionization 1.7 cm long in the z direction, i.e., the drift direction. In fig. 9, we show some typical drift paths of the ionization electrons created along such a particle trajectory, represented by the dashed lines. The higher electric field within the wire cell causes saturation and a reduction in the drift velocity [10]. We took the 5 cm/μs mentioned in the reference as the drift velocity around the sense wire, where the electric field was high, because it was not possible to make an actual measurement. The path with minimum total drift time determines which portion of the ionization actually initiates the wire signal. To simplify the calculation a straight-line approach was used to determine the fastest path. By straight-line approach we mean that once the drift electrons pass the pulsing grid plane, they go straight toward the sense wire with constant drift velocity, as indicated in the figure by solid arrows pointing towards the sense wire. This approximation ignores changes in drift velocity and the displacements due to the $E \times B$ effect as the drift electrons get closer to the sense wire.

The primary ionization electrons produced by the high-energy charged particle along its trajectory are randomly distributed because of the statistical nature of its interactions with the gas molecules. The primary ionizations result in secondary ionizations, which then drift toward the readout plane. The average number of primary ionization electrons was only about 20 per cm for the gas mixture used; therefore, the total ionization was not uniformly distributed. The nonuniformity, known as clustering, caused some uncertainty in locating the ionization electrons responsible for the wire signal. In the Monte Carlo simulation, this effect was taken into account by a smearing based on the average clustering distance of about 500 μm.

Once the location of the first arriving ionization cluster along the projected track was decided upon, the Monte Carlo code gave the corresponding three-dimensional coordinates. If the associated sense wire was along the x direction, the y coordinate was set to the y coordinate of the sense wire. If the orientation was in the y direction, on the other hand, the x coordinate of the sense wire was used. No attempt was made to simulate the actual individual cathode pad signals.

3.5. Magnetic field nonuniformity

The entire magnetic field of the spectrometer was measured and was shown to have sufficient nonuniformity to require some correction. A plot of the z component of the magnetic field is given in fig. 10. The uniformity was quite good – about 0.1% – over the central active volume, but it deteriorated somewhat beyond a radius of 25 cm. To deal with this problem, we used a magnetic field map in the Monte Carlo simulation. The Runge–Kutta method was used to step the particle from one location to the next according to the local magnetic field.

The magnetic field map was stored in two 2-dimensional look-up tables, as a function of z and radial position. One table was used for the z-component field and the other for the radial component field. The field value at any location was obtained by interpolation. The cylindrical symmetry was apparent, as expected for a solenoid field. The actual variation around the circumference was less than 10 G in 6000.

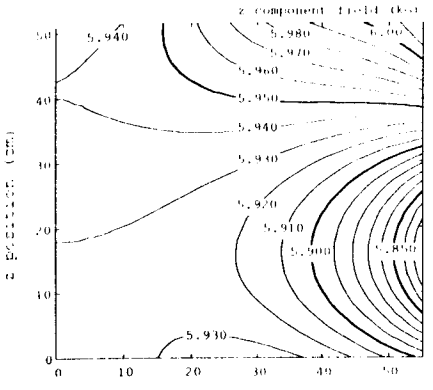

Fig. 10. Contour plot of the z component of the magnetic field showing the regions of nonuniformity.

3.6. Positive ion effect

In the course of comparing the Monte Carlo data with the experimental data, we realized that the latter were being distorted by a positive ion effect. The evidence is shown in fig. 11a, where the x–y projection of the coordinates in module 11 is shown for a helical track making just over one complete turn in the TPC. (The coordinates from the other modules were used in the fit but are not shown in the figure.) The solid curve represents the fitted helix. The arrow indicates the direction of positron momentum. Note that the points in the first portion of the trajectory, those which drifted the longest distance in the TPC, are shifted from the fitted helical path by as much as 0.5 cm. The z positions of these coordinates are shown in the y–z projection. In fig. 11b we show another event, which started in the opposite direction. Again, the points in the first portion of the track were displaced, but to the other side of the track. This phenomenon can be explained neither by the misalignment between electric and magnetic fields nor by the nonuniformity of the magnetic field. The Monte Carlo study indicated that the distortion could be accounted for to a large extent if one assumed that there was a positive space charge along the axis of the cylindrical drift region. Such a charge distribution would modify the electric field, causing an appreciable $E \times B$ effect on the drift electrons and a varying drift velocity within the drift volume.

We were able to obtain a substantial improvement in the comparison of *event topology*, i.e., the geometry of the positron trajectory, of the Monte Carlo result with that of the data by assuming the existence of a uniform positive charge density of 4.8×10^{-7} C/m^3 within a cylindrical volume having a 4 cm radius and extending through the entire length of the drift volume. An additional improvement was obtained by adding a second charge density of 3.4×10^{-8} C/m^3 within a cylindrical volume having a 45 cm radius. These charge distributions significantly modified the distribution of the electric field. The z component electric field at the center of the TPC, for example, was calculated to be about 135 V/cm at $z = 0$ and 190 V/cm at $z = 50$ cm, instead of a constant 160 V/cm. To take into account the space charge distributions, we used a numerical successive relaxation method [11] to calculate the electrical potential within the drift volume. The electric field was calculated from the potential distribution and used to estimate the $E \times B$ effects on the drift electrons.

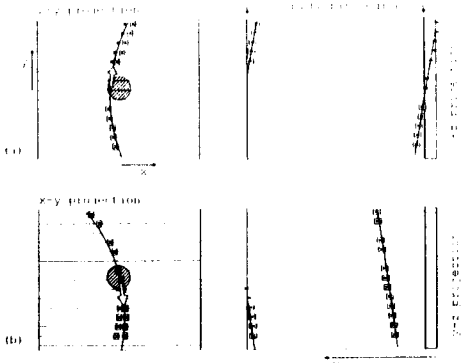

Fig. 11. Display of events showing evidence of the positive ion effect, i.e., the displacements for coordinates that drifted the longest distance in the TPC. The circle denotes the muon-stopping target. The ×'s are the observed coordinates. Only those enclosed in rectangles were used in the helix fit. The coordinates beyond the fiducial region were not used. In (a), the event started toward the positive y axis as seen in the x–y projection. The coordinates from the first portion of the track, the five boxed ×'s on the upper side of the x–y projection display, were displaced from the fitted helical path by the $E \times B$ force resulting from the positive ion effect. The y–z projection shows the z position of these coordinates. The rest of the boxed ×'s were of lower z position and consequently were not influenced as much by the $E \times B$ force. In (b), another event is shown, this time starting toward the negative y axis. The coordinates associated with high z position are now displaced to the left. The effect displayed here, together with other evidence, suggests the existence of the positive ion effect.

The resulting coordinate displacements were typically around 2 mm or less for most of the region. In the worst case, at radius $r = 4$ cm and $z = 51$ cm, the displacement amounted to 4.5 mm in the radial direction and 8.2 mm azimuthally. These results were incorporated in the look-up tables used to project the locations of the ionization electrons onto the readout plane. We also made an adjustment in the z position as described in section 4.5.

The avalanche process at the sense wire produces a large number of positive ions. A certain fraction of these positive ions passes through the grid plane and into the drift region, causing space charge problems [12]. The positive ions, moving at a speed of about 400 cm/s, will take more than 10 ms to clear the drift region. Ziock [13] estimated the number of positive ions caused, directly or indirectly, by the decay positron tracks. (By indirectly, we mean the subsequent production of positive ions during the avalanche process at the sense wires.) Taking into account the influence of the magnetic field on the trajectory, an avalanche gain of about 10^5, a transmission coefficient of 0.1 for the positive ions at the grounded grid, the mobility of the positive ions, and the incoming muon rate, the charge density turned out to be 3×10^{-9} C/m^3, averaged over the entire drift volume. In addition, there were the positive ions associated with the dark current of the wire chamber. This amounted to a space charge density of 18×10^{-9} C/m^3. The total, about 2.1×10^{-8} C/m^3, is within a factor of 2 of the second charge distribution used. In view of the uncertainties involved in the estimation, these numbers justified the choice we made.

The effect of a centralized positive ion distribution on the response of the TPC was observed in two instances during the experiment. First, for testing purposes, an intense beam of positrons was let into the TPC drift region. The amount of energy deposition at the center of the detector and the subsequent positive ion production were so large that a coordinate displacement as large as 7 cm in the z direction was recorded. Second, we noticed that a distortion also appeared whenever the separator was drawing about 40 μA of current between its positive and negative plates. Except in magnitude, these distortions were similar to what would be expected of the positive ion effect.

Our positive space charge distribution, within the 4 cm radius cylindrical column and at the center of the TPC, was believed to be caused by the X-rays produced at the separator, which drew about 6 μA of current under normal operation. Although the positive plate was located 5 cm below the beam line and two 3/4 inch diameter collimators were placed in the beam line, before and after the polarimeter, an aperture remained through which the X-rays were able to enter the TPC drift volume directly. The solid angle subtended by this aperture was about 4×10^{-6} sr. The efficiency of the X-ray generation was calculated using the equation given by Compton and Allison [14]:

$$\epsilon = \frac{\text{total X-ray energy}}{\text{total electron energy}} = 1.1 \times 10^{-9} ZV,$$

where Z is the atomic number of the element with which the electrons collide, and V is the voltage difference between the two electrodes. In our case, the efficiency ϵ was 1.1% with $Z = 26$ for iron and $V = 400\,000$ V. Assuming that the 6 μA of current was due entirely to the discharge between the negative and the positive plates of the separator and that the X-ray conversion occurred at 100% efficiency in the TPC, the resulting positive ion charge density in the TPC, after averaging over the 4 cm radius cylindrical column, was estimated to be about 1.6×10^{-4} C/m^3. This value, about 300 times the density of 4.8×10^{-7} C/m^3 used in the Monte Carlo simulation, is certainly an overestimate. In view of the fact that only a part of the 6 μA of separator current can be ascribed to the discharge current and that the X-ray conversion efficiency was actually far below 100%, we believe we have established the probable cause of the positive ion effect.

4. Analysis

The analyzer program used on the experimental data was also used to analyze the events generated by the Monte Carlo code to get the final momentum and angle values. Most of the hardware constraints were implemented at this stage. Fiducial cuts were applied wherever simulation of the actual data was not possible. The constraints applied to the Monte Carlo events are described in the paragraphs following.

4.1. Defects in the electronics

Defective electronics caused isolated dead regions within the TPC. All the bad electronics associated with the cathode pads and sense wires were flagged during the experiment. The corresponding dead regions were masked off in the analysis of both the actual and the simulated data.

The wire-signal amplifier-discriminator was designed to give an output signal that is updating and has a fixed width of about 600 ns. Because only one coordinate was produced regardless of the length of the signal, the amount of time the output stayed on became dead time for the sense wire. For tracks going flat with respect to the readout plane, this is very important. For each simulated event, a coordinate was removed if it was preceded in z position by other coordinates of the same wire by less than 5 cm, the equivalent of an 800 ns dead time.

4.2. Wire efficiencies

The wire analog signals were subject to fluctuations such as variations in the amount of ionization produced by the charged particle, gain variations from the avalanche process, and noise on the analog signal. All these factors contributed to the fluctuations in the analog signal pulse height and consequently to the inefficiency in the discriminator output. The wire-by-wire efficiency was recorded at the time the experimental data were analyzed and was used in the random elimination of coordinates for the Monte Carlo events.

4.3. Position resolution

We measured the position resolution of the TPC using tracks produced by high-energy cosmic rays. Because the effect of multiple scattering is minimal for very high-energy particles, the measured resolution is due primarily to diffusion of the ionization electrons, signal multiplication at the sense wire, and electronic noise. The overall resolution was found to be 0.9 mm along the sense wire and 1.3 mm in z. These values were used as the sigma of Gaussian distributions for randomly smearing out the coordinates of the simulated events.

4.4. Regions of uncertainty

The data from some regions of the TPC were not as good as those obtained from others. For example, the signal on the last cathode pad, at the end of each sense wire, appeared to be smaller than average. It was suspected that positive ions accumulating on the surface of the G-10 wire support structure were distorting the electric field. For both the experimental and the Monte Carlo data, coordinates within the last 1 cm of either end of the sense wire were removed. Another region of uncertainty was that where the particle trajectory crossed the wire at a very small angle. The segment of ionization, all of which falls inside the sensitive volume of one sense wire, can be as long as 10 cm. The result was a complicated signal pattern on the cathode pads, the analysis of which was difficult and unreliable. Coordinates with corresponding track-crossing angles of less than 30° or greater than 150° were used only in the track search, not in the final fit for the helix parameters.

4.5. Readjusting the z position

For the z-position calculation, as mentioned, we assumed a constant drift velocity. When the electric field becomes nonuniform, however, the drift velocity is no longer constant. The drift velocity as a function of the electric field had been measured at various electric field settings. With a given electric field distribution, the total drift time required for the ionization electrons to reach the readout plane could be calculated. The drift time was dependent on the location at which the ionization was created, but no longer a linear function of the z position. The result of the calculation was incorporated in a look-up table and was used to readjust the z position of the coordinates of each Monte Carlo event. The adjustment of the z coordinates was made at the analysis stage as a matter of convenience, aside from the fact that z coordinates are free from the geometrical constraints of the readout plane.

Although the z position corresponding to a wire crossing may occur anywhere along the trajectory, in practice the data were recorded on-line at intervals of 50 ns. The z position of the data was calculated using the time of wire turn-on. With the drift velocity at 6.8 cm/μs, the z position was measured only in increments of about 3.5 mm. This effect was also incorporated in the simulation. A study showed that there was no appreciable difference.

5. Results

5.1. The residuals

The accuracy of the Monte Carlo simulation can be judged by examining the reconstructed helix and the calculated residuals. This was mentioned earlier as the topology comparison. The residual is the amount each coordinate deviates from the value it would have if it were exactly on the fitted helix trajectory. Two types of residuals were studied, the z residual and the radial residual. Here, by radial we mean the direction going from the axis of the fitted helix toward the individual coordinate. The radial residual is the amount by which an individual coordinate deviates from the fitted helix circle when projected onto the x-y plane. Usually, the distributions of the residuals are expected to be centered around zero unless systematic distortions are present. For example, the nonuniform magnetic field changes the dip angle of a track as it spirals around. When such a trajectory is compared with an exact helix, the deviation can be a function of the z position. The deviations at various locations along the track are usually too small to be observed on each individual event. However, over a large ensemble of events the deviations can show up distinctly as distributions with nonzero centroids. An accurate Monte Carlo simulation would give distributions of residuals similar to those of the observed data. We chose to study the residuals as a function of the z position, i.e., z residual versus z and radial residual versus z. In both cases, we saw clearly a substantial improvement in the comparison of the distributions of residuals once we had taken into account the positive ion effect discussed in section 3.6.

The effect of the positive ions was most dramatic when the residuals of coordinates of module 11, only, were compared. Module 11 is located at the center of the readout plane. Fig. 12a shows, for module 11 only, how the radial residuals vary as a function of z, in this case for data and for Monte Carlo results with and without the positive ion effect. The topology of events chosen for the residual studies was such that the region above module 11 and around 40 cm in the z position was not reachable by the helical tracks; consequently, no data points are displayed. The radial residuals of coordinates from all modules except 11 are shown in fig. 12b. In fig. 13 the z residuals as a function of z are displayed. Again, (a) shows the z residuals of coordinates from module 11, only, and (b) those of coordinates from all other modules.

The improvement obtained by taking the positive ion effect into account was quite marked. In fact, it was this comparison that led us to realize the importance of the positive ion effect. The magnitude of the effect included in the simulation was estimated on the basis of this comparison. The comparison of residuals of coordinates from modules other than 11 also showed improvement,

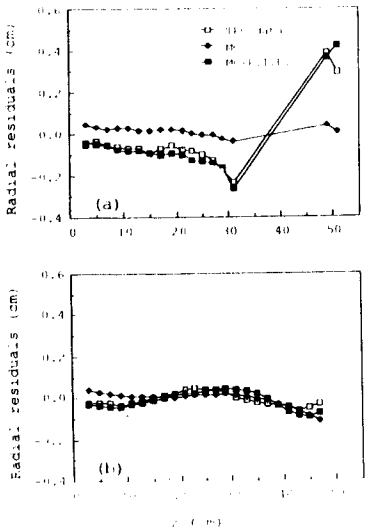

Fig. 12. The centroids of radial residual distributions at various positions (a) Radial residuals of module 11 coordinates only. (b) Radial residuals of coordinates from all modules other than module 11. The three curves are for the observed TPC data, Monte Carlo (MC), and Monte Carlo with the positive ion effect (PIE). The estimated errors on the calculated centroid were about the same size as the symbols used for displaying data points and were not plotted.

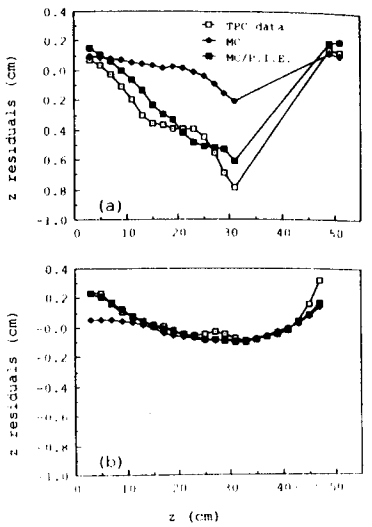

Fig. 13. The centroids of the z residuals at various z positions. Shown in (a) are the z residuals of coordinates from module 11 only and in (b) the z residuals for all coordinates except those of module 11. The three curves represent the data and Monte Carlo results with and without the positive ion effect.

although not as strikingly as that of module 11 alone. This may be taken as evidence that most of the positive ions are located in the central region of the TPC.

5.2. Momentum spectrum

A comparison of the momentum spectrum from the Monte Carlo estimate with the observed spectrum is shown in fig. 14. The spectra shown were obtained by summing over events in the angular range $-0.6 \leq \cos\theta \leq -0.3$. The solid curve is the Monte Carlo estimate in which ρ was given its canonical value of 0.75, with first-order radiative corrections to the spectrum included. The plotted points with errors displayed are from the observations. Neither curve can be described as smooth, and we consider it a victory that the Monte Carlo simulation succeeded in following the data as well as it did. A χ^2 per degree of freedom (DOF) of 2.9 was obtained from the comparison. Because a good fit should give a χ^2/DOF of about 1.0, the value we obtained implied the presence of a systematic error or, equivalently, an inadequacy in the simulation. An estimate of a lower limit to the magnitude of the systematic error may be obtained from the amount the statistical error would have to be augmented to bring the χ^2/DOF down to 1.0. Our value of 2.9 can be accounted for if

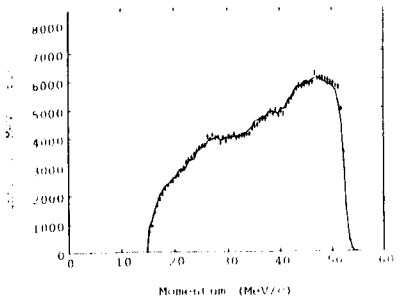

Fig. 14. Comparison of the observed momentum spectrum (points with error bars) with the Monte Carlo spectrum (solid curve), using $\rho = 0.75$ and summing over the cos θ range from -0.6 to -0.3.

the systematic error is ≥ 1.4 times the statistical error, assuming that the systematic error adds in quadrature to the statistical error. It should be pointed out that the value chosen for ρ could itself be the cause of systematic error. When we allowed the value of ρ to vary, we obtained a χ^2/DOF = 2.3 for a best fit to the spectrum. This represents an improvement, but the essential argument remains unchanged. Our estimate of the systematic error is given as a lower limit because we cannot be sure that the uncertainties of the fit are all statistical in character.

The discrepancies between the two spectra show up more readily when the ratio of data/Monte Carlo is

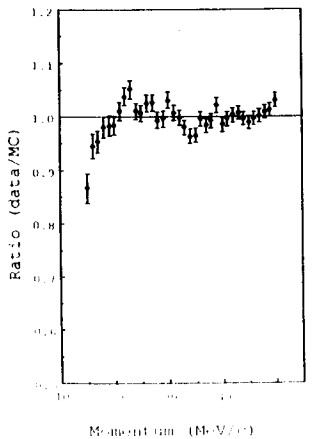

Fig. 15. Ratio of event counts, data over Monte Carlo, in every 1 MeV/c bin, as a function of momentum for the angular range $-0.6 \leq \cos\theta \leq -0.3$. The error bars indicate the statistical uncertainty.

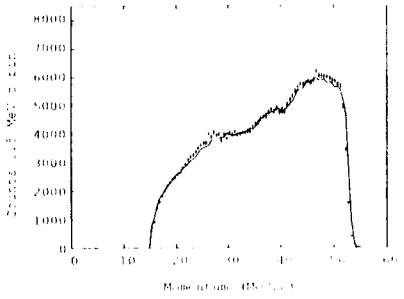

Fig. 16. Comparison of the observed spectrum (points with error bars) with the Monte Carlo spectrum with the positive ion effect not included (solid curve), using $\rho = 0.75$ and summing over the cos θ range from -0.6 to -0.3.

plotted over the smooth part of the spectrum (excluding the end point). This is shown in fig. 15. The agreement is generally good, but the discrepancy below 25 MeV/c is clearly outside the statistics and is believed to be due to systematic effects of unknown origin.

The importance of including the positive ion effect can be further demonstrated by comparing the same momentum spectra with the result of the Monte Carlo simulation without the positive ion effect, as shown in fig. 16. We obtained a χ^2/DOF = 15.3. The corresponding estimate of the lower limit for the systematic error was about 2.8 times as large as when the positive ion effect was included. A best fit to the ρ parameter yielded χ^2/DOF = 13.8, also significantly larger.

6. Conclusions

The results of the Monte Carlo simulation presented here is in good agreement with the observed data. The process of simulation included most of the known characteristics of the detector. Look-up tables were used extensively and efficiently in the implementation of various corrections to the simulated coordinates or trajectories that would otherwise have required a major computational task. The topology comparison in which the coordinate residuals were used turned out to be a powerful means for obtaining insight into either the accuracy of the simulation or the detector systematics. The subsequent adjustment made to the simulation, as a result of the comparison, is believed to cause no bias in the intended physics analysis toward a specific physics result. The study of the residuals demonstrated unmistakably the existence of a positive ion effect. The improvement in the spectrum comparison obtained by taking this effect into account is considered an independent confirmation of the existence of the positive ion

fect. The model used for the positive ion distribution as good enough to provide significant improvements. n the other hand, enough discrepancy remains to ggest the need for a better and more realistic model, if final analysis for a physics result were to be atmpted.

cknowledgements

I am grateful to my sponsor, Prof. H.L. Anderson, r the support and advice he gave me during the course this work, to Dr. W.W. Kinnison, for the way in hich he conducted the experiment and for his support uring the data analysis process, to Dr. R.J. McKee ho developed the essential data analysis software, and Dr. H.J. Ziock for many useful discussions. I also ank the other members of the muon-decay experient: J.W. Lillberg, C.E. Milner, A. Zehnder, D. Bowan, C.K. Hargrove, and T. Suzuki. I appreciate the pport of the National Science Foundation, through ant No. PHY 86-01628 to the University of Chicago, nd of the Department of Energy, through Los Alamos ational Laboratory.

ppendix
cceptance-resolution function

To derive the acceptance-resolution function we keep bs on the initial conditions of each Monte Carlo vent. That along with the final conditions – the final tted positron track – will give us the resolution funcon. The acceptance will automatically be contained in he resolution because some of those initial conditions ill not lead to final conditions.

The quantities below are used to represent the physial parameter of the decay positron:

μ = reduced momentum and cos(dip angle).
= azimuthal angle of the positron momentum as it leaves the decay point.
ξ = starting position of the positron orbit in the target.

Let t symbolize the final topology (what we get by oing the final fit, if we get anything at all) and t' ymbolize the initial topology (what the positron has mmediately after leaving the decay point). The quantity is determined for each event by the uniform roll of he dice

$x', \mu', \phi', \zeta', \xi'$.

x, μ, ϕ, ζ, ξ

The resolution function can be written as follows:

$\mathcal{R}(x', \mu', \phi', \zeta', \xi', x - x', \mu - \mu', \phi - \phi', \zeta - \zeta', \xi - \xi') = R(\text{args})$.

This function is simply the probability that if we start with a topology t' we will end up with a topology t. In many cases we may end up with no final topology at all. In other words, for certain t and t', $R(\text{args}) = 0$. $R(\text{args})$ is not normalized to 1. The integral of $R(\text{args})$ over all t is just the acceptance for t'.

If we choose some distribution of muons in the target $T(\zeta', \xi')$ – which later we take to be uniform – and assume an azimuthal symmetry in the ϕ angle of the muon-decay spectrum, we can integrate over target and azimuth variables.

$$P(x', \mu', x - x', \mu - \mu') = \int_{-\pi}^{\pi} d\phi' \int_{-\pi}^{\pi} d\phi \int\int_T d\zeta' \, d\xi' \int\int_{-\infty}^{\infty} d\zeta \, d\xi R(\text{args}) \times T(\zeta', \xi').$$

Incorporating the bare Michel spectrum $M(x', \mu')$, i.e., the theoretical decay positron spectrum, leads to an expression for the expected Monte Carlo spectrum:

$$D(x, \mu) = \int_0^{\infty} dx' \int_{-1}^{1} d\mu' \times P(x', \mu', x - x', \mu - \mu') M(x', \mu').$$

We now assume that the acceptance-resolution function is symmetric in the argument $\mu - \mu'$. This assumption is true in general if no systematic effect is involved. Because the range of μ in which we are interested is far enough away from ± 1, the probability function $P(x', \mu', x - x', \mu - \mu')$ is practically zero at the integration boundary. In this case it is possible to simplify our formula further by integrating over the μ':

$$D(x, \mu) = \int_0^{\infty} M(x', \mu) \, dx' \times \int_{-1}^{1} P(x', \mu', x - x', \mu - \mu') \, d\mu'.$$

We have used $M(x', \mu)$ in the formula instead of $M(x', \mu')$ to take advantage of the symmetry of the acceptance-resolution function in the argument $\mu - \mu'$. If we now define the new acceptance-resolution function as

$$P(x', x - x', \mu) = \int_{-1}^{1} P(x', \mu', x - x', \mu - \mu') \, d\mu'.$$

we have a simplified formula for the theoretical spectrum to which we fit the observed spectrum.

$$D(x, \mu) = \int_0^{\infty} P(x', x - x', \mu) M(x', \mu) \, dx'.$$

This formula is much easier to use because for each final x and μ we have to know only about the initial momentum x'.

It is more practical to do the comparison between the Monte Carlo spectrum and the observations by binning the data. We define binds for a given x' with

index k. Every uniform roll of the dice will drop a count in one of these bins.

N_k = number of counts of all the Monte Carlo events with their initial momenta within the range covered by bin k.

n_{kij} = number of counts whose initial topology puts the event in bin k and whose final topology puts the event in bin ij. The bins in x and μ of the final topology are denoted by i and j.

Note that because not every event of initial topology will end up with a final topology, i.e., it may be lost, we have the following inequality:

$$N_k \geq \sum_{ij} n_{kij}.$$

Thus, the resolution function is simply

$$P(x'_k, x_i - x'_k, \mu_j) = n_{kij}/N_k \equiv P_{kij}.$$

To get the Monte Carlo counts in the bin ij, we must integrate the Michel function, $M(x, \mu)$ with radiative corrections included, over the dimensions of bin k:

$$D(x_i, \mu_j) = \sum_k P_{kij} \int_{\text{bin } k} M(x', \mu_j) \, dx'.$$

The value of $D(x_i, \mu_j)$ depends on the value chosen for the Michel parameter ρ, which is imbedded inside the expression $M(x', \mu_j)$. The value of this parameter can be determined by a comparison with the observed spectrum. We calculate chi-squared by comparing the observed counts with the Monte Carlo counts in each bin. The parameter ρ is determined by finding the value of this parameter that gives χ^2 its minimum value. The actual binning sizes used are 0.5 MeV/c in the final momentum, 0.01 in cos θ of the dip angle, and 0.25 MeV/c in the original momentum.

References

[1] N. Marx and D.R. Nygren, Phys. Today (Oct. 1978) 46.
[2] H.L. Anderson, Los Alamos National Laboratory report LA-7893-C (1979).
[3] W.W. Kinnison, AIP Conf. Proc. 108, ed. J.A. Macdonald (1983) p. 21.
[4] J.W. Lillberg, Nucl. Instr. and Meth. A240 (1985) 122.
[5] A. Breskin, G. Charpak, C. Demierre, S. Majewski, A. Policarpo, F. Sauli and J.C. Santiard, Nucl. Instr. and Meth. 143 (1977) 29.
[6] R.J. McKee, AIP conf. Proc. 108, ed. J.A. Macdonald (1983) p. 242.
[7] W.R. Nelson, H. Hirayama and D.W.O. Rogers, The EGS4 Code System, SLAC Report 265 (1985).
[8] Proposal for a PEP Facility Based on the Time Projection Chamber, D.R. Nygren spokesman, PEP Experiment no. 4, SLAC PUB-5012 (1976) appendix 9.
[9] C.K. Hargrove et al., Nucl. Instr. and Meth. 219 (1984) 461.
[10] F. Sauli, CERN 77-09 (1977) 22.
[11] M. DiStasio and W.C. McHarris, Am. J. Phys. 47 (1979) 440.
[12] D. Friedrich, G. Melchart, B. Sadoulet and F. Sauli, Nucl. Instr. and Meth. 158 (1979) 81.
[13] H.J. Ziock, private communication.
[14] A.H. Compton and S.K. Allison, X-Rays in Theory and Experiment (D. Van Nostrand, New York, 1949) p. 90.